Precipitation driving of droplet concentration variability in marine low clouds

Robert Wood,[1] David Leon,[2] Matthew Lebsock,[3] Jefferson Snider,[2] and Antony D. Clarke[4]

Received 25 June 2012; revised 8 August 2012; accepted 8 September 2012; published 11 October 2012.

[1] The concentration N_d of cloud droplets in marine low clouds is a primary determinant of their ability to reflect sunlight and modulates their ability to precipitate. Previous studies have focused upon aerosol source variability as the key driver of variability in N_d. Here, we use a highly simplified aerosol budget model to examine the impact of precipitation on N_d. This model considers: precipitation (coalescence) scavenging, constrained using new satellite measurements of light precipitation; entrainment of aerosol from above cloud combined with constant aerosol concentration based on recent field observations of aerosol particles in the free troposphere; and sea-surface aerosol production estimated using a wind speed dependent source function. Despite the highly simplified nature of this model, it skillfully predicts the geographical variability of N_d in regions of extensive marine low clouds. Inclusion of precipitation results in reduction in N_d by factors of 2–3 over the remote oceans. Within 500 km of coastlines the reduction in N_d due to precipitation is weak but in these regions the model is not able to accurately predict N_d because of strong pollution sources. In general, neither free-tropospheric nor surface CCN sources alone are sufficient to maintain N_d against precipitation losses. The results demonstrate that even the light precipitation rates typical of marine stratocumulus profoundly impact the radiative properties of marine low clouds.

Citation: Wood, R., D. Leon, M. Lebsock, J. Snider, and A. D. Clarke (2012), Precipitation driving of droplet concentration variability in marine low clouds, *J. Geophys. Res.*, *117*, D19210, doi:10.1029/2012JD018305.

1. Introduction

[2] Anthropogenic activities have resulted in marked increases in the concentration of aerosol particles in the atmosphere [*Kaufman et al.*, 2002; *Isaksen et al.*, 2009] and these increases exert a significant but highly uncertain radiative forcing on the global climate [*Isaksen et al.*, 2009; *Intergovernmental Panel on Climate Change*, 2007]. A large fraction of this forcing is attributed to the effects that aerosol particles have on clouds by increasing the concentration N_d of cloud droplets [*Martin et al.*, 1994; *Ramanathan et al.*, 2001; *Lohmann and Feichter*, 2005], reducing droplet size [*Bréon et al.*, 2002], thereby increasing the reflected solar radiation [*Twomey*, 1974; *Penner et al.*, 2004; *Quaas et al.*, 2009]. Systematic increases in N_d have been observed downwind of east Asia over the past two decades [*Bennartz et al.*, 2011] and have been attributed to rapid industrialization. The magnitude of the so-called "aerosol indirect effect" on climate depends not only upon present-day conditions, but also upon the unperturbed microphysical state of the clouds prior to the addition of anthropogenic aerosols [*Platnick and Twomey*, 1994; *Oreopoulos and Platnick*, 2008]. It is reasonable to argue that N_d is the single most important cloud microphysical variable that must be accurately represented in models in order to accurately determine aerosol indirect effects on climate. However, there are marked differences between values of N_d in different climate models [*Quaas et al.*, 2009; *Ming et al.*, 2006; *Gettelman et al.*, 2008] demonstrating a clear lack of understanding of the key controls on N_d.

[3] Satellite-based studies use the relationship between observed cloud droplet size or concentration, and nearby clear-sky estimates of aerosol loading, to infer the role that aerosols play in influencing clouds and climate [*Bréon et al.*, 2002]. Some even go so far as to quantitatively estimate aerosol indirect effects globally [*Quaas et al.*, 2008; *Jones et al.*, 2009]. Inherent in this approach is that correlations between cloud microphysical properties and aerosols in the current climate are indicative of an aerosol influence on

[1]Department of Atmospheric Sciences, University of Washington, Seattle, Washington, USA.
[2]Department of Atmospheric Sciences, University of Wyoming, Laramie, Wyoming, USA.
[3]Jet Propulsion Laboratory, California Institute of Technology, Pasadena, California, USA.
[4]Department of Oceanography, University of Hawai'i at Manoa, Honolulu, Hawaii, USA.

Corresponding author: R. Wood, Department of Atmospheric Sciences, 408 ATG Building, University of Washington, Seattle, WA, 98195-1640, USA. (robwood@atmos.washington.edu)

0148-0227/12/2012JD018305

cloud properties rather than vice versa. Aerosol-cloud correlative studies do not take the possible effects of precipitation into account. One can make a reasonable case that precipitation-induced aerosol changes will not significantly impact the inferences drawn from these studies only if one assumes that the impacts of precipitation are localized, intermittent, and relatively rare, and that the aerosol fields that interact with the majority of clouds are not significantly affected by precipitation. However, recent observations from the sensitive spaceborne radar on the CloudSat satellite are finding that precipitation occurs more frequently over the globe than previously thought [*Leon et al.*, 2008; *Haynes et al.*, 2009] prompting an examination of the role of precipitation in driving aerosol variability.

[4] In this study we use these state-of-the-art quantitative estimates of light precipitation from CloudSat to constrain a simple budget model that predicts the mean concentrations of cloud condensation nuclei (CCN) and cloud droplets over those parts of the global oceans containing extensive low clouds. These clouds are confined within the marine boundary layer (MBL) and are among the most susceptible to aerosol perturbations [*Oreopoulos and Platnick*, 2008]. We build upon previous studies [*Baker and Charlson*, 1990; *Baker*, 1993] that used simplified budget models to provide important insights into the factors controlling CCN, by constructing a steady state budget for CCN in the MBL appropriate for the regions of large-scale subsidence where extensive marine stratocumulus clouds are favored [*Klein and Hartmann*, 1993].

[5] This article is organized as follows. Section 2 describes the basis for a simple, single-equation, steady state budget model to predict CCN or N_d in the MBL. Section 3 describes how we determine the terms in the budget using a variety of observations including satellites and in situ data. Section 4 presents the key results from the model and compares the model against satellite observations of N_d. Section 5 discusses the implications of our findings.

2. Steady State Budget Model

[6] The rate of increase of CCN concentration $\dot{N}$ averaged over the depth of the MBL can be written as the sum of various source and sink terms:

$$\dot{N} = \dot{N}_{FT} + \dot{N}_S + \dot{N}_{PROD} + \dot{N}_P + \dot{N}_{DRY} + \dot{N}_{ADV} \qquad (1)$$

where $\dot{N}_{FT}$, $\dot{N}_S$, $\dot{N}_{PROD}$, $\dot{N}_P$, $\dot{N}_{DRY}$ and $\dot{N}_{ADV}$ are the time tendencies due to entrainment of CCN from the free-troposphere (FT), primary production at the surface (i.e. sea spray), and secondary production, precipitation (i.e. coalescence scavenging), dry deposition to the surface and horizontal advection, respectively.

[7] Free-tropospheric air is constantly being mixed into the MBL by cloud top entrainment, and this can either provide a net source of CCN to the MBL or can dilute MBL aerosol concentrations. Modeling and observational studies suggest that the FT is a primary source of CCN in the remote MBL [*Clarke et al.*, 1998a; *Capaldo et al.*, 1999; *Katoshevski et al.*, 1999]. The net source rate is $\dot{N}_{FT} = w_e(N_{FT} - N)/z_i$ where z_i is the depth of the MBL and w_e is the entrainment rate.

[8] The modeled surface source $\dot{N}_S$ is assumed to be from primary production of sea-spray aerosol (SSA) and we use a recent parameterization [*Clarke et al.*, 2006] to provide $\dot{N}_S = F(\sigma)U_{10}^{3.41}/z_i$ where U_{10} is the wind speed at a height of 10 m, and $F(\sigma)$ depends upon the assumed peak supersaturation σ experienced in the clouds (see section 3.1 below). We examine the sensitivity to the parameterization of sea-spray by comparing with the frequently used formulation of *Monahan et al.* [1986]. Since this formulation has the same wind speed dependence as *Clarke et al.* [2006], the expression for $\dot{N}_S$ given above is identical for the two schemes, but the function $F(\sigma)$ is different. We discuss how the supersaturation and $F(\sigma)$ are specified in Sections 3.1 and 3.3 below.

[9] The model does not take into account CCN formation from the nucleation of new particles in the MBL since it is unlikely that this contributes significantly to the mean CCN number concentration over the oceans. In severely scavenged ultraclean MBLs evidence of new particle formation has been noted [*Clarke et al.*, 1998b; *Petters et al.*, 2006; *Tomlinson et al.*, 2007; *Wood et al.*, 2008]. Such nucleation events appear to be quite rare, with only one clear instance observed during four weeks of shipborne sampling over the tropical southeastern Pacific Ocean [*Tomlinson et al.*, 2007]. In addition, evidence that freshly nucleated particles can grow to sufficient sizes to increase the population of CCN without being scavenged by existing cloud is lacking. Nucleation events are therefore unlikely to compete with other source processes in determining the mean state [*Capaldo et al.*, 1999; *Katoshevski et al.*, 1999]. In any case, formulations for the rate of production of CCN from new particle formation in the MBL are highly uncertain [*Capaldo et al.*, 1999; *Kirkby et al.*, 2011]. To maintain simplicity, and because the production rates are highly uncertain, we do not include production of CCN from other secondary processes like aqueous phase processing. We therefore set the secondary production rate $\dot{N}_{PROD} = 0$.

[10] The precipitation sink term $\dot{N}_P$ depends upon the precipitation rate at cloud base P_{CB}. We use a formulation that accounts for losses from the collection of cloud droplets by precipitation drops in the cloud via accretion [*Wood*, 2006]. This gives $\dot{N}_P = K\,N\,P_{CB}\,h/z_i$, where $K = 2.25\ m^2\ kg^{-1}$ is a constant that depends upon the collection efficiency of cloud droplets by drizzle drops [*Wood*, 2006], and h is the cloud thickness.

[11] Dry deposition of CCN to the ocean is estimated using deposition velocity parameterization [*Giorgi*, 1988] for accumulation mode particles (0.05–1 μm diameter) that make up the bulk of the CCN in the MBL. Rates are in the range 0.001–0.01 cm s^{-1} with the higher values occurring at higher wind speeds and for the larger of the accumulation mode particles. Given these deposition velocities, we find that dry deposition constitutes only a very weak sink for CCN under most circumstances, with loss rates unlikely to exceed 2 $cm^{-3}\ d^{-1}$ for most values of N observed, and most wind speeds, over the oceans. We are therefore justified in setting $\dot{N}_{DRY} = 0$ in the budget model.

[12] We also set $\dot{N}_{ADV} = 0$ to avoid the complication of calculating spatial gradients and to facilitate the interpretation of the key physical processes controlling N_d. It is possible to estimate the magnitude of the advection term $\dot{N}_{ADV}$ using the observed cloud droplet concentration from satellite [*George and Wood*, 2010]. Over the remote oceans the

magnitude of $\dot{N}_{ADV}$ is generally 10 cm^{-3} d^{-1} or less, while higher values can be found in near-coastal regions. Including advection in the steady state model introduces an additional level of complexity since it involves taking spatial gradients. To preserve simplicity we omit it from the model. Since precipitation is the dominant control on N_d in the model, the geographic pattern of the advection term largely follows the spatial gradient in precipitation rate.

[13] In this study we examine the time-mean CCN budget by setting $\dot{N} = 0$ in equation (1) inserting the expressions discussed above for the various terms, and rearranging to obtain an expression for the steady state value N_{eq} of the CCN concentration in the MBL as

$$N_{eq} = \frac{\left(N_{FT} + \frac{F(\sigma)U_{10}^{3.41}}{Dz_i}\right)}{\left(1 + \frac{hKP_{CB}}{Dz_i}\right)} \quad (2)$$

[14] Here we have also assumed that entrainment is in balance with the large-scale subsidence rate, so that $w_e = D\, z_i$,. where D is the large scale divergence, appropriately assumed to be constant with height over the depth of the MBL [*Wood et al.*, 2009]. In practice, the entrainment rate exceeds the subsidence rate by 10–40% over the subtropical stratocumulus regions [*Wood and Bretherton*, 2004], but estimating its precise value is itself a major challenge [*Stevens*, 2002] and is not attempted here.

3. Model Constraints and Inputs

[15] The CCN budget model (equations (1) and (2)) implicitly assumes that the cloud droplet concentration N_d and the CCN concentration are one and the same. This is reasonable provided that (a) we choose an appropriate peak supersaturation σ in order to convert the aerosol sources, which are provided as a function of aerosol size, into tendencies of CCN; (b) the cloud droplet concentration throughout the cloud is equal to that determined by the aerosol activation process.

3.1. Supersaturation

[16] For marine stratocumulus clouds, observations suggest that values of σ in the range 0.1–0.8% are typical with mean values around 0.3% consistent with observations [*Martin et al.*, 1994; *Snider et al.*, 2003]. Here we assume a constant value of $\sigma = 0.3\%$ for all calculations. The peak supersaturation $\sigma = 0.3\%$ assumed in the model is assumed to be constant everywhere. Understanding how this changes systematically over the remote oceans is complex, as it depends upon variations in the strength of the turbulent updrafts and upon the size distribution of the aerosol being activated [*Martin et al.*, 1994; *Snider et al.*, 2003]. We use recent field measurements of mean aerosol size distributions at different distances from the Chilean coast from the VOCALS Regional Experiment (REx) [*Wood et al.*, 2011] to estimate the likely systematic geographical variability in σ. In the marine boundary layer, the Hoppel minimum [*Hoppel et al.*, 1986] in the size distribution is indicative of the minimum size of aerosols that are activated. Assuming a hygroscopic aerosol, this minimum size is directly related to the supersaturation. A systematic reduction from 0.1 to 0.07 μm in the minimum diameter was observed to occur from 70°W to 78°W moving westward along 20°S away from the Chilean coast [*Kleinman et al.*, 2012]. This implies that the mean supersaturation increases by ~60% from the coast offshore. However, the coastal CCN concentrations are high consistent with pollution aerosol impacts [*Allen et al.*, 2011], and so these are not representative of the supersaturations we are attempting to represent in the model. No systematic shift in the Hoppel minimum is observed over the cleaner region from 74°W to 78°W, suggesting that systematic changes in supersaturation over the remoter regions may be considerably smaller than occur near the coasts.

3.2. Free-Tropospheric CCN

[17] We constrain N_{FT} based on aerosol measurements from field data taken in the Southern and Northern Hemisphere remote subtropical FT. Two data sources are used:

[18] 1. The first source is aircraft measurements of FT CCN from a thermal diffusion CCN counter taken on the NSF/NCAR C-130 aircraft during the VOCALS-REx. Details of the instrument are provided in *Snider et al.* [2006], and flight plans are described in *Wood et al.* [2011] A total of 638 CCN measurements were made in the FT (61, 117, 147 and 313 at supersaturations of approximately 0.1, 0.25, 0.5 and 0.9% respectively) along the 20°S latitude line from the coast (70°W) to approximately 1500 km offshore (85°W) over the month-long campaign. CCN concentrations are corrected to an assumed mean MBL pressure of 925 hPa, which is the typical pressure at which clouds form in the region [*Bretherton et al.*, 2010].

[19] 2. The second source is a composite time-mean size distribution measured over 17 days with large scale subsidence at a remote FT station on Mauna Loa during July 1992. These data are described in *Weber and McMurry* [1996] and are also corrected to a pressure of 925 hPa. We convert the size distribution into a CCN spectrum using a plausible range of aerosol hygroscopicity following the 'kappa' parameter approach [*Petters and Kreidenweis*, 2007]. A reasonable lower boundary ($\kappa = 0.3$) is approximately the lowest value of CCN-based hygroscopicity measured in the northeastern Pacific FT from *Roberts et al.* [2010]. The upper boundary ($\kappa = 0.98$) is the geometric mean value from *Roberts et al.* [2010]. Values of κ significantly higher than unity were inferred from CCN measurements in *Roberts et al.* [2010] but seem implausible given that even the most hygroscopic compounds have κ values of about unity [*Petters and Kreidenweis*, 2007]. Ammonium sulfate has a κ value of approximately 0.7 [*Petters and Kreidenweis*, 2007].

[20] Figure 1a compares the measured CCN concentrations in the southeastern Pacific FT with those from Mauna Loa. For the southeastern Pacific, we take data from west of 75°W (>500 km off the Chilean coast) that is minimally impacted by coastal pollution [*Allen et al.*, 2011]. Time-mean CCN concentrations west of 75°W over the southeastern Pacific Ocean (Figure 1) are in remarkably good agreement with those derived from the Mauna Loa size distribution measurements. This is perhaps surprising because although the southeastern Pacific and Hawaii are in similar tropical meteorological regimes, one might expect marked differences in the mean size distribution due to the different array of sources and landmasses in the Northern and Southern Hemisphere. The mean distributions are made

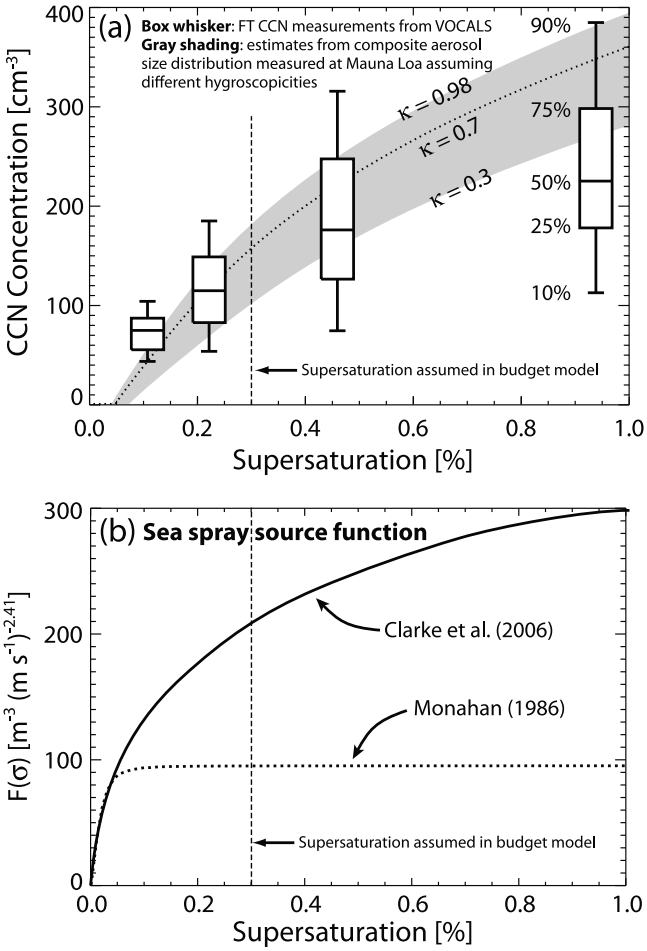

Figure 1. (a) Free-tropospheric CCN spectra from the southeastern Pacific and Hawaii. Observations from the southeastern Pacific are from CCN spectra taken in the remote FT west of 75°W using the NSF/NCAR C-130 aircraft in VOCALS-REx [*Wood et al.*, 2011], corrected to an assumed mean MBL pressure of 925 hPa. Box-whisker plots show the 10th, 25th, 50th, 75th, and 90th percentile concentrations for four supersaturations. Shaded region shows a plausible range of CCN concentration estimated using the composite size distribution for subsiding FT air measured on Mauna Loa in Hawaii [*Weber and McMurry*, 1996], corrected to an assumed mean MBL pressure of 925 hPa, with the spread representing a plausible range of hygroscopicity κ parameters [*Petters and Kreidenweis*, 2007] for clean FT air (see text). (b) Sea-spray source functions $F(\sigma)$ as a function of supersaturation, for the *Clarke et al.* [2006] parameterization used in this study, and from *Monahan et al.* [1986] for comparison.

up of a mixture of different aerosol populations from a number of different sources. Previous studies [*Clarke et al.*, 1998a; *Friedlander*, 1977; *Raes*, 1995] suggest that new particle formation from naturally produced sulfuric acid in the upper troposphere constitutes one major source of clean FT CCN. This aerosol subsequently subsides in the descending branches of large scale atmospheric systems where its distribution is expected to reach a quasi-steady state [*Friedlander*, 1977; *Raes*, 1995]. In addition, the remote marine FT also includes air masses transported long distances from continents that likely contain some pollution aerosol.

[21] We derive a value of N_{FT} in the range 100–175 cm^{-3} active at σ = 0.3% from the mean Mauna Loa size distribution (assuming a plausible range of aerosol hygroscopicity, see caption, Figure 1a). This is in good agreement with longitude-correlated CCN (0.2 to 0.5%) and total non-volatile concentrations made in the FT during VOCALS (see Figure 2a and Methods section). For the model base case we therefore assume a constant mean concentration N_{FT} = 125 cm^{-3} everywhere, which is within 20% of the time-mean values derived from the remote subtropical data in

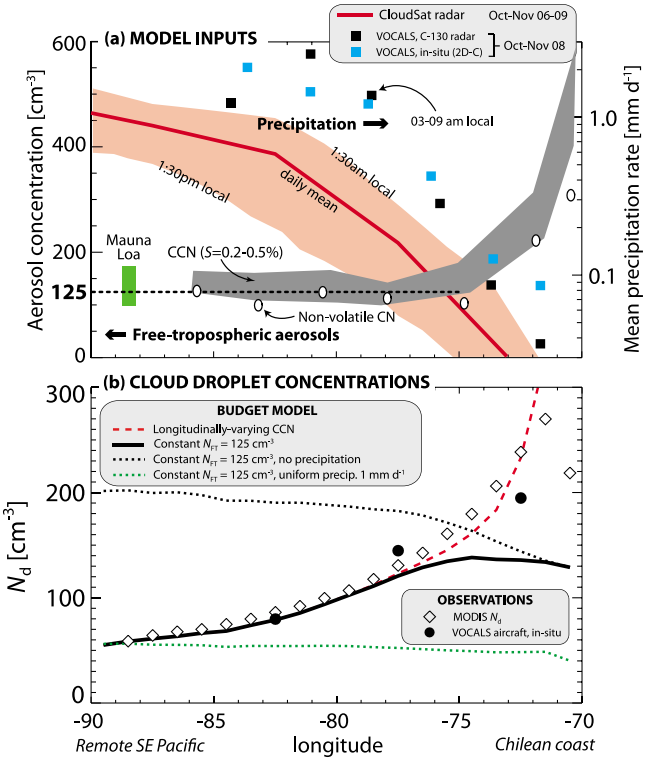

Figure 2. Model inputs and results from southeastern Pacific stratocumulus region from 70 to 90°W along 20°S. (a) Free-tropospheric (FT) aerosol concentrations (left axis) showing range of mean CCN concentrations corresponding to supersaturations relevant for cloud formation (gray shading), and total non-volatile particle concentration (open circles). Green bar shows estimated CCN for 0.2–0.5% supersaturation from measurements of FT aerosol size distributions during subsiding conditions on Mauna Loa, Hawaii, see the Methods section; cloud base precipitation rates (right axis) estimated from CloudSat satellite (mean for October/November 2006–2009 between 22°S and 18°S, red shading showing 1:30 am and 1:30 pm local time overpasses) and from the VOCALS-REx field experiment (black and blue squares from aircraft radar and in situ precipitation probes respectively, in the latitude range 18–22°S). (b) Observed (solid circles: aircraft during VOCALS [*Bretherton et al.*, 2010; *Wood et al.*, 2011], diamonds: satellite estimates from MODIS, 18–22°S) and modeled mean cloud droplet concentration N_d for different model scenarios as denoted in legend and discussed in the text.

both hemispheres. We also force the model with observed values of FT CCN from VOCALS-REx and conduct additional sensitivity tests, as described in Section 4.

3.3. Sea Surface Source

[22] For the surface source, we use a size-resolved sea spray generation function [*Clarke et al.*, 2006] to estimate the rate of particle generation for particles active at $\sigma = 0.3\%$ supersaturation. This is determined numerically by integrating the size-resolved surface source function from the largest particles down to the critical dry diameter for a given supersaturation. This provides a supersaturation-dependent $F(\sigma)$ curve shown in Figure 1b. For $\sigma = 0.3\%$ the critical diameter is 50 nm, which yields a value of 214 m^{-3} $(m\ s^{-1})^{-2.41}$ for $\sigma = 0.3\%$ (Figure 1b). For a wind speed of 8 m s^{-1} this yields $\dot{N}_S = 22\ cm^{-3}\ d^{-1}$ averaged over an MBL that is 1 km deep. The widely used source function of *Monahan et al.* [1986] has the same wind speed dependence but a rate that is over a factor of two lower (Figure 1b).

[23] To drive SSA production we use daily mean wind speed estimates from the QuikScat satellite and average the production rates up to monthly averages. Including sub-daily timescale variability in wind speed increases the surface production of SSA, but we find from reanalysis data that including 6 hourly estimates increases SSA production by less than 10%.

3.4. Precipitation Sink

[24] The model sink term is driven by new precipitation rate estimates from the profiling W-band radar on the CloudSat satellite [*Lebsock and L'Ecuyer*, 2011]. The cloud base precipitation rate needed to calculate the coalescence scavenging [*Wood*, 2006] is estimated as the maximum value in each radar profile. Mean precipitation rates from low clouds are estimated for $5 \times 5^\circ$ grid boxes globally by removing profiles with detectable echoes above the 3 km level. For the regions considered, the results are not strongly sensitive to the choice of this level since the majority of the clouds are situated below 2 km. Gridded precipitation rates are produced on a monthly basis for data from 2006 to 2009.

[25] We also use precipitation measurements from VOCALS-REx to compare against those from CloudSat. For this, we use both aircraft in situ observations from an optical array probe, and aircraft radar measurements from the University of Wyoming Cloud Radar. The VOCALS-REx precipitation data set is described in *Bretherton et al.* [2010]. The majority of the aircraft flights were conducted during the later part of the night (03–09 local time) when precipitation rates are at their diurnal maximum.

3.5. Boundary Layer Depth, Cloud Thickness, Wind Speed, and Surface Divergence

[26] Equation (2) indicates that we also need to estimate MBL depth z_i, cloud thickness h, surface wind speed U_{10}, and surface divergence D. MBL depth is estimated using from MODIS cloud top temperature retrievals [*Wood and Bretherton*, 2004]. Cloud thickness h is estimated with an adiabatic assumption [e.g., *Albrecht et al.*, 1990] using MODIS retrievals of cloud liquid water path (LWP). This relationship is $h = (2LWP/\Gamma)^{1/2}$, where Γ is a weak function of temperature and pressure [*Albrecht et al.*, 1990], evaluated as described in *Wood and Bretherton* [2004]. Both cloud top temperature and LWP are taken from $1 \times 1^\circ$ gridded daily Level 3 MODIS products. The results are not strongly sensitive to these parameters. Wind speed and surface divergence estimates are from the QuikScat satellite (see *Wood et al.* [2009] for details).

3.6. Cloud Droplet Concentration

[27] Satellite estimates of cloud droplet concentration are used to compare against model-derived N_{eq} from equation (2). Model estimates are produced globally on a $1 \times 1^\circ$ grid on a month by month basis. Cloud droplet concentration estimates from the Moderate Resolution Imaging Spectroradiometer (MODIS) on the NASA Terra satellite are produced from daily Level 3 data for $1 \times 1^\circ$ boxes using a visible/near infrared approach [*Bennartz*, 2007]. To minimize problems of retrievals in broken clouds, we only include in our averages those daily boxes where the cloud cover from liquid clouds exceeds 0.8. These are then averaged together to provide monthly mean N_d estimates.

3.7. Model Estimates of N_d

[28] We use the budget model equation (2) to predict monthly mean values of N_d by forcing with monthly mean values of the input variables discussed above. Annual means are then derived from the monthly means only for those months with (a) mean subsidence (positive mean surface divergence); (b) mean boundary layer depth shallower than 4 km; and (c) with mean liquid cloud fractions exceeding 0.3. Annual mean data are only analyzed for those locations where at least four months pass the acceptance criteria.

4. Results

4.1. Model Assessment Over the Southeastern Pacific

[29] To assess the quality of the model, we use recent field measurements from VOCALS-REx that extensively sampled the lower troposphere over the tropical southeastern Pacific Ocean [*Wood et al.*, 2011]. The measurements focused upon characterizing the largest semi-permanent subtropical sheet of stratocumulus on Earth that extends westward from the Chilean and Peruvian coasts. Extensive survey sampling was carried out along 20°S from the Chilean coast at 70°W to ~1400 km offshore at 85°W using a combination of different research aircraft. Measurements were made in both the MBL and the lower FT. Figure 2a shows observations of the two key inputs to the budget model, namely the time-mean FT CCN concentration (section 3.2) and the precipitation rate close to the cloud base (section 3.4). CCN concentrations in the FT fall off sharply within 500 km of the coast but, despite considerable day to day variability, the time-mean campaign values remain relatively constant for over 1000 km out to 85°W (Figure 2a). Several lines of evidence point to anthropogenic pollution being responsible for the high values very close to the coast [*Allen et al.*, 2011; *Yang et al.*, 2011; *Saide et al.*, 2012].

[30] The cloud base precipitation rate increases markedly with distance from the Chilean coast, from an essentially nonprecipitating state with <0.1 mm d^{-1} near the coast to >1 mm d^{-1} at 85°W (Figure 2a). Rates of a few tenths of a mm d^{-1} are sufficient to drive significant coalescence scavenging of CCN [*Feingold et al.*, 1996; *Wood*, 2006]. This gradient in precipitation is driven to a significant extent

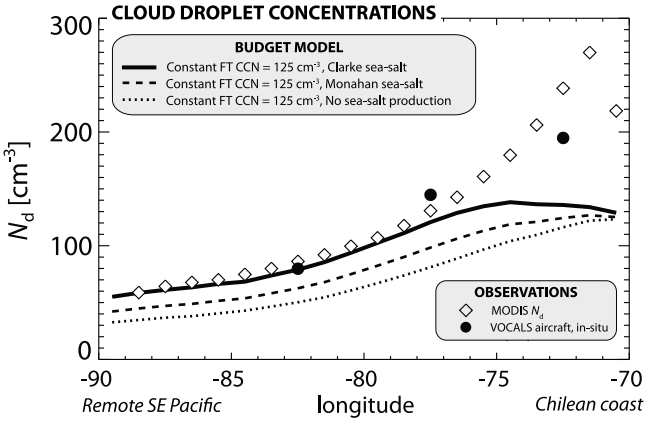

Figure 3. Effects of different assumptions regarding primary production of sea-salt in the model. Same as Figure 2b, but showing sensitivity to sea-salt aerosol parameterization used. Observed (solid circles: aircraft during VOCALS (taken from *Bretherton et al.* [2010]), diamonds: satellite estimates from MODIS, 18–22°S) and modeled mean cloud droplet concentration N_d. Solid line: standard model set up with constant FT CCN. Dashed line: Monahan sea-salt parameterization [*Monahan et al.*, 1986] in place of *Clarke et al.* [2006]. Dotted line: No primary production of sea-salt at all.

by thickening clouds and a deeper boundary layer to the west [*Bretherton et al.*, 2010], but is likely also modulated by aerosol in the MBL [*Terai et al.*, 2012]. The cause of the precipitation is not the focus of this study. Precipitation production in marine stratocumulus maximizes at night [*Leon et al.*, 2008], and is typically heaviest in the early morning hours when the clouds are at their thickest [*Bretherton et al.*, 2004; *Wood et al.*, 2002]. This is apparent in the observations where precipitation rates are lowest at 1:30 pm (CloudSat, daytime overpass, Figure 2a), take intermediate values at 1:30 am (CloudSat nighttime overpass) and are largest during 03–09 A.M. (VOCALS field data). Since the timescale for CCN removal due to precipitation is typically at least 1 day given these precipitation rates [*Wood*, 2006], we use a daily mean estimate as the mean of the two CloudSat overpasses to drive the model.

[31] The model, when forced with CloudSat observed mean precipitation rates and observed FT CCN, captures the observed increase in N_d as the coast is approached (Figure 2b) with remarkable fidelity given the model's simplicity. The model predicts a factor of two increase in N_d from 90°W to 75°W even when the model is forced with a fixed FT CCN concentration of 125 cm^{-3} (consistent with mean values over the remote region away from the coast). With fixed CCN, however, the model is unable to reproduce the highest concentrations within 500 km of the coast (Figure 2b). However, these high values are obtained when the model is forced with the observed longitudinally varying FT CCN concentration increase that includes the near-coastal enhancement due to pollution sources [*Allen et al.*, 2011] (Figure 2b). The general behavior of decreasing N_d westward from 75 to 90°W is caused by increasing precipitation scavenging (Figure 2a), which can be seen by comparing the model estimates with fixed FT CCN and either no precipitation or precipitation fixed at a constant value of 1 mm d^{-1} (Figure 2b). A critical finding here is that a precipitation rate of as little as 1 mm d^{-1} is sufficient to drive down N_d by a factor of three over the remote ocean, which further serves to emphasize how important precipitation from low clouds is in controlling mean cloud droplet concentrations over the remote ocean.

[32] Primary production from sea-spray constitutes a weaker, but nevertheless significant, source than entrainment from the FT consistent with a previous study with the same parameterization [*Clarke et al.*, 2006]. However, it is important to note that we are using a source function that is one of the more prolific available [*de Leeuw et al.*, 2011], although experimentation with different primary production parameterizations only changes the modeled N_d values by less than 20% (Figure 3). The CCN concentration from sea-spray (the difference between the solid and the dotted line in Figure 3) ranges from <10 cm^{-3} close to the Chilean coast, where wind speeds are low, to around 40 cm^{-3} further afield, where wind speeds are higher. These findings are consistent with preliminary measurements of sea-salt particles from aircraft during VOCALS-REx (Anthony Clarke, personal communication). The choice of sea-spray parameterization does not affect our conclusions regarding the importance of precipitation at driving the offshore gradient in cloud droplet concentration over the southeastern Pacific.

4.2. Application to Marine Low Cloud Regions Globally

[33] Given the ability of the budget model with fixed FT CCN concentrations to reproduce with some skill the gradient in N_d over the remote southeastern Pacific Ocean (more than 500 km from the coast), we apply the model more generally to regions of extensive marine low cloud under conditions of large scale subsidence (Figure 4). Aerosol concentrations in the FT vary significantly both regionally and in response to variations in natural and anthropogenic sources [*Allen et al.*, 2011]. Because there are no global observational constraints on the time-mean FT CCN, we draw on the consistency between mean FT CCN spectra at Mauna Loa and over the southeastern Pacific Ocean (Figure 1 and section 3.2) and fix N_{FT} = 125 cm^{-3} everywhere for the base case. The satellite observations show that N_d values in excess of 150 cm^{-3} tend to be located near the continental coastlines (e.g., California, Chile/Peru, Europe), with values reducing toward the remote oceans, where they are as low as 30–60 cm^{-3} (Figure 4, top). The base case model is able to reproduce well the mean values (Table 1) and geographical variability in N_d (Figure 4) for low cloud regions, especially for the remote subtropical/tropical regions 35°S–35°N. The model underestimates N_d close to coastlines (Table 1) consistent with a lack of continental sources. The model also captures the low values (<60 cm^{-3}) over the remote North Pacific and Atlantic and the Southern Ocean north of 45°S. Removing the precipitation sink increases mean N_d in the model by a factor of 2–3 over the remote oceans, but only 15% in the near-coastal regions where precipitation rates are very low (Table 1). A doubling of N_{FT} from 80 to 160 cm^{-3} leads to a 50–70% increase in N_d (Table 1) because FT CCN is partly buffered by surface sources.

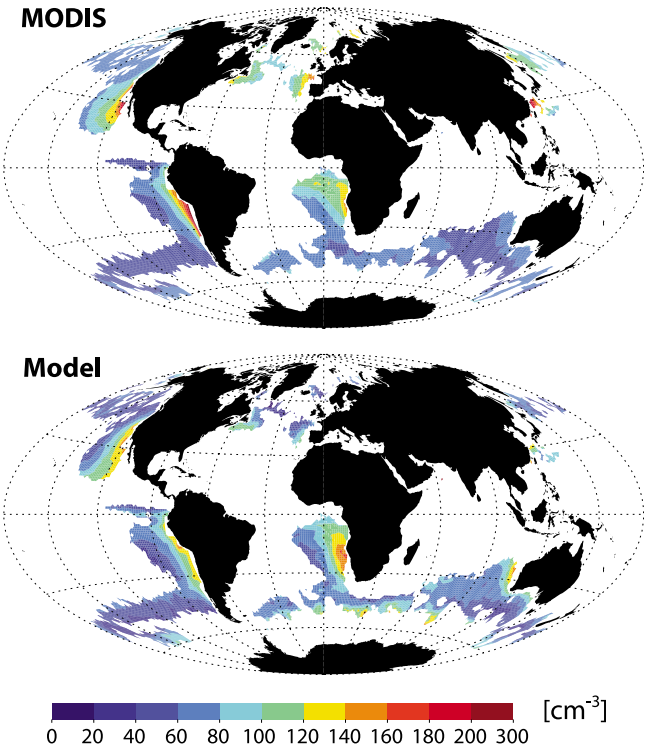

Figure 4. Cloud droplet concentrations in regions of extensive marine low clouds observed by satellite and from the budget model. Annual mean cloud droplet concentration N_d for extensive marine low clouds under conditions of large scale subsidence, (top) from MODIS (see Methods section); (bottom) from the CCN budget model for the same regions.

[34] The skill of the base case model in predicting N_d variability is remarkable given that there is no variation whatsoever in the FT CCN source in Figure 4. To examine the key factors controlling the geographical variability of N_d in the model, we conduct additional model sensitivity experiments. In each experiment, only one (or two) of the variables in equation (2) is allowed to vary. All other variables are fixed by setting them to their respective mean values over time and space (Table 2). It is clear that precipitation variability is required in order to produce the strong correlation with observations seen in the base case (r = 0.65). No other variable can alone explain more than 15% of the observed geographical variance in N_d. Divergence and cloud thickness variations also lead to model fields with significant positive correlations (r = 0.21 and 0.37 respectively), but the geographical variability in N_d driven by these variables is far too weak to explain the observed variability (Table 2). The correlations are positive because divergence and cloud thickness correlate quite well with precipitation itself. We find that wind speed variability alone explains an insignificant amount of the model N_d variability (r = −0.06), from which we conclude that variability in SSA is not a significant contributor to the observed geographical variability in N_d. This is especially true in the subtropics and tropics where wind speeds are relatively modest and the FT source is greater than the surface source (Figure 5). However, SSA does contribute to the mean N_d (Table 1) despite not substantially impacting its geographical variability.

Table 1. The Effects on the Mean Cloud Droplet Concentration in Various Geographical Regions of Changing the Primary Source and Sink Terms

	Mean Cloud Droplet Concentration (cm^{-3})		
Observed or Model Estimate	35°S–35°N	35°S–35°N Within 300 km of Coastlines	60°S–60°N
Observations (MODIS)	88	152	74
Model, base case (N_{FT} = 125 cm^{-3})	88	129	74
Model, N_{FT} = 0	20	21	25
Model, no SSA	68	109	46
Model, no precipitation	169	150	245
Model, N_{FT} = 80 cm^{-3}	63	90	55
Model, N_{FT} = 160 cm^{-3}	107	154	85

Table 2. Geographical Variability of Cloud Droplet Concentration for Various Model Configurations[a]

Model Configuration	r (obs, model)	$\sigma_{model}/\sigma_{obs}$
Base case	0.65	0.92
P_{CB} variability only	0.77	1.01
P_{CB} and U_{10} variability only	0.70	0.97
U_{10} variability only	*−0.06*	0.37
D variability only	0.21	0.18
h variability only	0.37	0.13
z_i variability only	−0.32	0.10

[a]Results show correlation coefficients between annual mean MODIS observed and model estimates of annual mean N_d and the ratio of the model and observed standard deviations ($\sigma_{model}/\sigma_{obs}$). Correlations not significant at the 2σ level are italicized. All results are for the tropics and subtropics (35°S–35°N).

[35] Overall, these results lead us to argue that a large fraction of the observed geographical variability in cloud droplet concentration in extensive marine low clouds over the remote oceans is driven by precipitation losses rather than aerosol source variability. This is further demonstrated by noting the striking similarities between the maps of the mean observed precipitation rates from low clouds (Figure 6) and the observed N_d field (Figure 4, top).

[36] Frequency distributions of monthly mean N_d (Figure 7) show that the base case model (N_{FT} = 125 cm^{-3}) can represent satellite-observed N_d variability well. As we might expect from Figure 2, the model is unable to capture the very highest concentrations observed by the satellite (N_d > 200 cm^{-3}) that are mostly regions within a few hundred kilometers of coastlines. This is because neither the advection of continentally influenced MBL air nor elevated near-coastal FT concentrations (e.g., Figure 2) are considered in the model. When the model is forced by removing either FT CCN or SSA production, the model is unable to represent the distribution of observed N_d and underestimates the mean N_d (Figure 7 and see also Table 1). This further emphasizes that the surface and FT are both important contributors to the cloud droplet concentration over the remote oceans [*Katoshevski et al.*, 1999; *Capaldo et al.*, 1999;

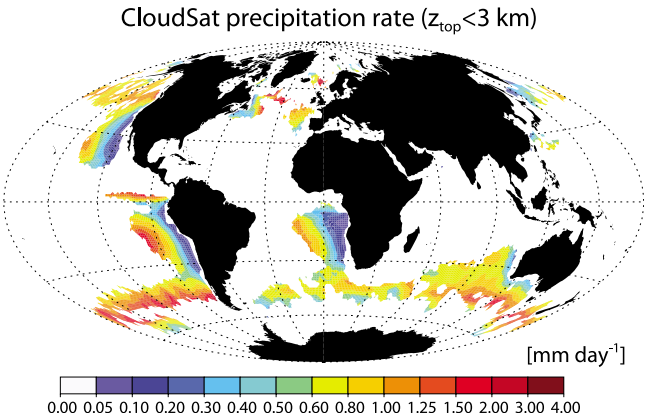

Figure 5. Mean precipitation rate at cloud base from low clouds (cloud top height z_{top} < 3 km) estimated with spaceborne radar measurements from CloudSat [*Lebsock and L'Ecuyer*, 2011]. Data are screened to display regions of extensive marine low clouds under conditions of mean subsidence as in Figure 4.

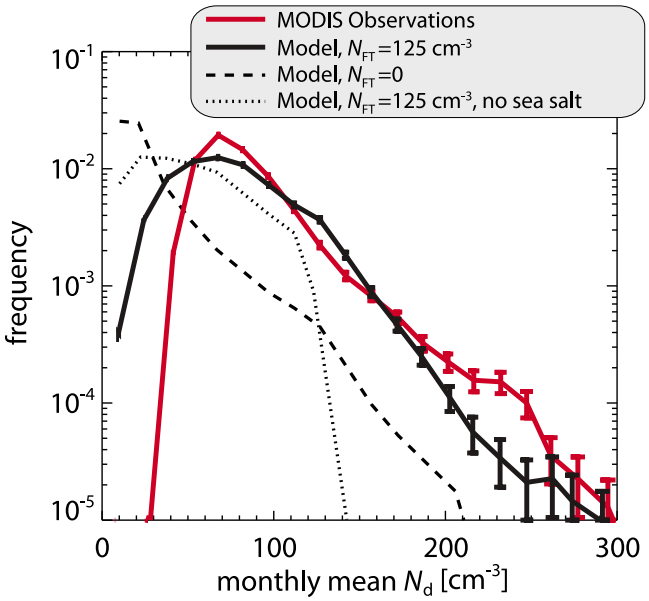

Figure 7. Frequency distributions of observed and modeled monthly mean cloud droplet concentration. Only months that meet the criteria needed to contribute to the means shown in Figure 4 (regions with extensive low clouds under divergent conditions) are shown. Shown here are the base version of the model (i.e., that used to construct Figure 4, solid black), together with estimates with no FT contribution to CCN (dashed), and no sea salt contribution (dotted). Error bars show the 95% confidence interval in the frequency estimates for the observations and for the model base case due to sampling limitations.

Clarke et al., 2006]. The shape of the model N_d distribution is relatively insensitive to plausible variations in the assumed mean FT CCN concentration (Figure 8).

5. Implications and Conclusions

[37] Our results have a number of important implications. First, if CCN and cloud droplet concentration variability over much of the global ocean are determined by precipitation variability rather than aerosol source variability, this calls into question the interpretation of correlative studies [*Quaas et al.*, 2008; *Jones et al.*, 2009] linking cloud properties to aerosol

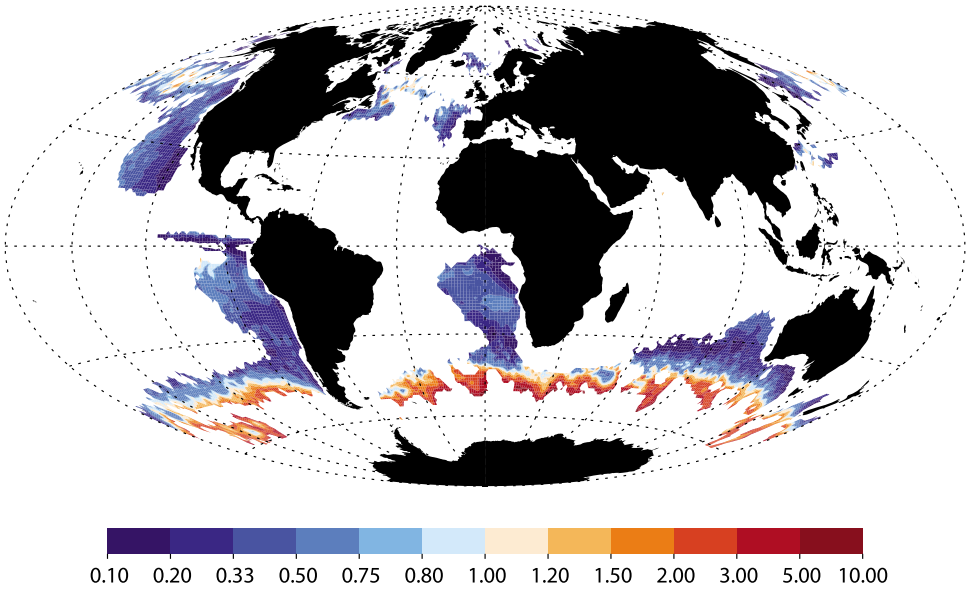

Figure 6. Ratio of CCN flux from surface to that from entrainment from the free troposphere (FT) in the model. The FT CCN concentration is set to 125 cm^{-3} and the surface source depends upon daily wind speed. In the subtropics and tropics, the majority of the CCN originate from the FT, but in the midlatitudes where winds are stronger, the surface source can exceed that from the FT.

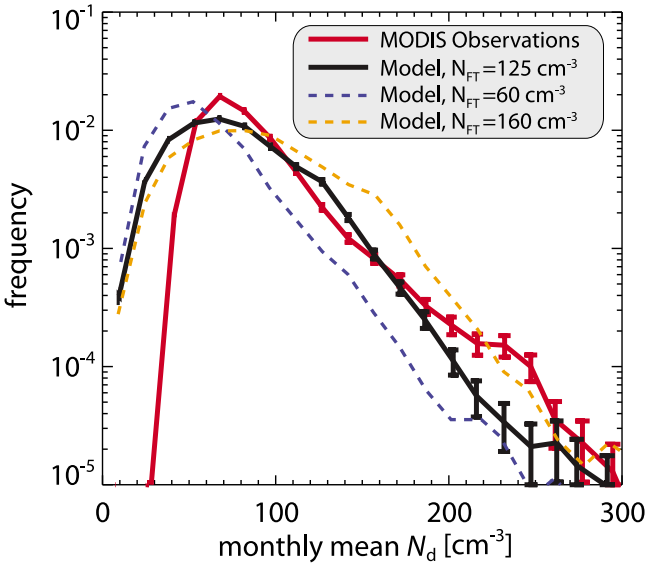

Figure 8. Sensitivity to assumed free tropospheric CCN concentration N_{FT} of the frequency distributions modeled monthly mean cloud droplet concentration. Only months that meet the criteria needed to contribute to the means shown in Figure 4 (regions with extensive low clouds under divergent conditions) are shown. Shown here are the base version of the model (i.e., that used to construct Figure 4, solid black), together with model estimates with low (N_{FT} = 80 cm^{-3}) and high (N_{FT} = 160 cm^{-3}) estimates of the FT contribution to CCN (dashed blue and orange respectively). Error bars show the 95% confidence interval in the frequency estimates for the observations and for the model base case due to sampling limitations.

properties as providing useful information on anthropogenic aerosol indirect effects on climate. It also suggests that the notion of there being a 'background' aerosol concentration in the unperturbed marine boundary layer may not be a useful one because MBL CCN concentrations are strongly modulated by precipitation processes that vary strongly both geographically and temporally. The FT CCN over remote oceanic regions is known to reflect a complex mixture of different sources, some of which are natural and some anthropogenic [*Clarke and Kapustin*, 2010]. Our finding that a constant time-mean FT CCN supply is sufficient to explain a significant fraction of the time-mean gradients in the cloud droplet concentration over the remote oceans should not therefore be interpreted as indicating that the remote oceanic regions are devoid of anthropogenic influence. The increasing concentrations observed within about 500 km of continents most likely reflects a lower tropospheric pathway for the transport of continental aerosols to the MBL, whereas the more remote anthropogenic contributions are associated with aerosol or precursors lofted higher into the troposphere that can then be transported long distances before subsidence carries them into the MBL.

[38] Here we have shown that MBL cloud droplet concentrations are impacted by precipitation generated by the clouds themselves, but we note that an increasing body of evidence shows that precipitation in low clouds typically decreases with cloud droplet concentration [*Stevens and Feingold*, 2009]. There is then the potential for a significant positive feedback whereby modest increases in CCN reduce the precipitation sink, amplifying the initial perturbation. Although we do not claim evidence for bistability in the system [*Baker and Charlson*, 1990], our results do suggest that pollution-driven CCN increases may be amplified by precipitation suppression and that this warrants further exploration with more sophisticated models. There is modeling evidence for this in the recent literature [*Yang et al.*, 2012].

[39] Finally, we note that climate models tend to impose arbitrary fixed limits on cloud droplet concentration minima [*Quaas et al.*, 2009] suggesting deficiencies in modeling the processes responsible for low concentrations over the remote ocean. Across models, there is a significant correlation between this fixed lower limit on N_d and the strength of the aerosol indirect effect [*Quaas et al.*, 2009]. A closer focus on the role of precipitation is therefore needed to better understand whether climate models are able to produce light precipitation in the marine boundary layer, and whether the model aerosols are impacted appropriately by it. This study helps to highlight that we now have the satellite measurements of light precipitation and cloud microphysical properties to begin to explore this critical control on cloud microphysical properties. Further work could include an examination of the effects of seasonal precipitation variability on the seasonal cycle of cloud droplet concentration, as suggested by previous work [*Liu*, 2010].

[40] **Acknowledgments.** The authors would like to thank the staff and crew of the NSF/NCAR C-130 aircraft whose dedication resulted in the in situ observational VOCALS Regional Experiment data set. The CloudSat data were distributed by the CloudSat Data Processing Center at Colorado State University. MODIS data were obtained from the NASA Goddard Land Processes data archive. QuikScat data were produced by Remote Sensing Systems and sponsored by the NASA Ocean Vector Winds Science Team. This work was supported by NASA awards NNX10AN78G and NNX10AM29G and NSF awards ATM-0745702, ATM-0745368 and ATM-0745986. Part of this research was carried out at the Jet Propulsion Laboratory, California Institute of Technology, under a contract with the National Aeronautics and Space Administration.

References

Albrecht, B. A., C. W. Fairall, D. W. Thomson, A. B. White, J. B. Snider, and W. H. Schubert (1990), Surface-based remote-sensing of the observed and the adiabatic liquid water content of stratocumulus clouds, *Geophys. Res. Lett.*, *17*, 89–92, doi:10.1029/GL017i001p00089.

Allen, G., et al. (2011), South East Pacific atmospheric composition and variability sampled along 20°S during VOCALS-REx, *Atmos. Chem. Phys.*, *11*, 5237–5262, doi:10.5194/acp-11-5237-2011.

Baker, M. B. (1993), Variability in concentrations of cloud condensation nuclei in the marine cloud-topped boundary layer, *Tellus, Ser. B*, *45*, 458–472.

Baker, M. B., and R. L. Charlson (1990), Bistability of CCN concentrations and thermodynamics in the cloud-topped boundary layer, *Nature*, *345*, 142–145, doi:10.1038/345142a0.

Bennartz, R. (2007), Global assessment of marine boundary layer cloud droplet number concentration from satellite, *J. Geophys. Res.*, *112*, D02201, doi:10.1029/2006JD007547.

Bennartz, R., J. Fan, J. Rausch, L. R. Leung, and A. K. Heidinger (2011), Pollution from China increases cloud droplet number, suppresses rain over the East China Sea, *Geophys. Res. Lett.*, *38*, L09704, doi:10.1029/2011GL047235.

Bréon, F. M., D. Tanre, and S. Generoso (2002), Aerosol effect on cloud droplet size monitored from satellite, *Science*, *295*, 834–838, doi:10.1126/science.1066434.

Bretherton, C. S., T. Uttal, C. W. Fairall, S. E. Yuter, R. A. Weller, D. Baumgardner, K. Comstock, and R. Wood (2004), The EPIC 2001 Stratocumulus Study, *Bull. Am. Meteorol. Soc.*, *85*, 967–977.

Bretherton, C. S., R. Wood, R. C. George, D. Leon, G. Allen, and X. Zheng (2010), Southeast Pacific stratocumulus clouds, precipitation and boundary layer structure sampled along 20°S during VOCALS-REx, *Atmos. Chem. Phys.*, *10*, 10,639–10,654, doi:10.5194/acp-10-10639-2010.

Capaldo, K. P., P. Kasibhatla, and S. N. Pandis (1999), Is aerosol production within the remote marine boundary layer sufficient to maintain observed concentrations?, *J. Geophys. Res.*, *104*, 3483–3500, doi:10.1029/1998JD100080.

Clarke, A. D., and V. Kapustin (2010), Hemispheric aerosol vertical profiles: Anthropogenic impacts on optical depth and cloud nuclei, *Science*, *329*, 1488–1492, doi:10.1126/science.1188838.

Clarke, A. D., J. L. Varner, F. Eisele, R. L. Mauldin, D. Tanner, and M. Litchy (1998a), Particle production in the remote marine atmosphere: Cloud outflow and subsidence during ACE 1, *J. Geophys. Res.*, *103*(D13), 16,397–16,409, doi:10.1029/97JD02987.

Clarke, A. D., et al. (1998b), Particle nucleation in the tropical boundary layer and its coupling to marine sulfur sources, *Science*, *282*, 89–92, doi:10.1126/science.282.5386.89.

Clarke, A. D., S. R. Owens, and J. Zhou (2006), An ultrafine sea-salt flux from breaking waves: Implications for cloud condensation nuclei in the remote marine atmosphere, *J. Geophys. Res.*, *111*, D06202, doi:10.1029/2005JD006565.

de Leeuw, G., E. L. Andreas, M. D. Anguelova, C. W. Fairall, E. R. Lewis, C. O'Dowd, M. Schulz, and S. E. Schwartz (2011), Production flux of sea spray aerosol, *Rev. Geophys.*, *49*, RG2001, doi:10.1029/2010RG000349.

Feingold, G., S. M. Kreidenweis, B. Stevens, and W. R. Cotton (1996), Numerical simulations of stratocumulus processing of cloud condensation nuclei through collision-coalescence, *J. Geophys. Res.*, *101*, 21,391–21,402, doi:10.1029/96JD01552.

Friedlander, S. K. (1977), *Smoke, Dust and Haze*, John Wiley, Hoboken, N. J.

George, R. C., and R. Wood (2010), Subseasonal variability of low cloud radiative properties over the southeast Pacific Ocean, *Atmos. Chem. Phys.*, *10*, 4047–4063, doi:10.5194/acp-10-4047-2010.

Gettelman, A., H. Morrison, and S. J. Ghan (2008), A new two-moment bulk stratiform cloud microphysics scheme in the Community Atmosphere Model, Version 3(CAM3). Part II: Single-column and global results, *J. Clim.*, *21*, 3660–3679, doi:10.1175/2008JCLI2116.1.

Giorgi, F. (1988), Dry deposition velocities of atmospheric aerosols as inferred by applying a particle dry deposition parameterization to a general circulation model, *Tellus, Ser. B*, *40*, 23–41, doi:10.1111/j.1600-0889.1988.tb00210.x.

Haynes, J. M., T. S. L'Ecuyer, G. L. Stephens, S. D. Miller, C. Mitrescu, N. B. Wood, and S. Tanelli (2009), Rainfall retrieval over the ocean with spaceborne W-band radar, *J. Geophys. Res.*, *114*, D00A22, doi:10.1029/2008JD009973.

Hoppel, W. A., G. M. Frick, and R. E. Larson (1986), Effects of nonprecipitating clouds on the aerosol size distribution in the marine boundary layer, *Geophys. Res. Lett.*, *13*, 125–128, doi:10.1029/GL013i002p00125.

Intergovernmental Panel on Climate Change (2007), *Climate Change 2007: The Physical Science Basis. Contribution of Working Group I to the Fourth Assessment Report of the Intergovernmental Panel on Climate Change*, edited by S. Solomon et al., Cambridge Univ. Press, Cambridge, U. K.

Isaksen, I. S. A., et al. (2009), Atmospheric composition change: Climate–chemistry interactions, *Atmos. Environ.*, *43*, 5138–5192, doi:10.1016/j.atmosenv.2009.08.003.

Jones, T. A., S. A. Christopher, and J. Quaas (2009), A six year satellite-based assessment of the regional variations in aerosol indirect effects, *Atmos. Chem. Phys.*, *9*, 4091–4114, doi:10.5194/acp-9-4091-2009.

Katoshevski, D., A. Nenes, and J. H. Seinfeld (1999), A Study of processes that govern the maintenance of aerosols in the marine boundary layer, *J. Aerosol Sci.*, *30*, 503–532, doi:10.1016/S0021-8502(98)00740-X.

Kaufman, Y., D. Tanré, and O. Boucher (2002), A satellite view of aerosols in the climate system, *Nature*, *419*, 215–223, doi:10.1038/nature01091.

Kirkby, J., et al. (2011), Role of sulphuric acid, ammonia and galactic cosmic rays in atmospheric aerosol nucleation, *Nature*, *476*, 429–433, doi:10.1038/nature10343.

Klein, S. A., and D. L. Hartmann (1993), The seasonal cycle of low stratiform clouds, *J. Clim.*, *6*, 1587–1606, doi:10.1175/1520-0442(1993)006<1587:TSCOLS>2.0.CO;2.

Kleinman, L. I., et al. (2012), Aerosol concentration and size distribution measured below, in, and above cloud from the DOE G-1 during VOCALS-REx, *Atmos. Chem. Phys.*, *12*, 207–223, doi:10.5194/acp-12-207-2012.

Lebsock, M. D., and T. S. L'Ecuyer (2011), The retrieval of warm rain from CloudSat, *J. Geophys. Res.*, *116*, D20209, doi:10.1029/2011JD016076.

Leon, D. C., Z. Wang, and D. Liu (2008), Climatology of drizzle in marine boundary layer clouds based on 1 year of data from CloudSat and Cloud-Aerosol Lidar and Infrared Pathfinder Satellite Observations (CALIPSO), *J. Geophys. Res.*, *113*, D00A14, doi:10.1029/2008JD009835.

Liu, Y. (2010), Comments on "Seasonal variation of the physical properties of marine boundary layer clouds off the California coast," *J. Clim.*, *23*(12), 3416–3420, doi:10.1175/2010JCLI3407.1.

Lohmann, U., and J. Feichter (2005), Global indirect aerosol effects: A review, *Atmos. Chem. Phys. Discuss.*, *5*, 715–737.

Martin, G. M., D. W. Johnson, and A. Spice (1994), The measurement and parameterization of effective radius of droplets in warm stratocumulus clouds, *J. Atmos. Sci.*, *51*, 1823–1842, doi:10.1175/1520-0469(1994)051<1823:TMAPOE>2.0.CO;2.

Ming, Y., V. Ramaswamy, L. J. Donner, and V. T. J. Phillips (2006), A new parameterization of cloud droplet activation applicable to general circulation models, *J. Atmos. Sci.*, *63*, 1348–1356, doi:10.1175/JAS3686.1.

Monahan, E. C., D. E. Spiel, and K. L. Davidson (1986), A model of marine aerosol generation via whitecaps and wave disruption, in *Oceanic Whitecaps and Their Role in Air-Sea Exchange Processes*, edited by E. C. Monahan and G. Mac Niocaill, pp. 167–174, Springer, New York.

Oreopoulos, L., and S. Platnick (2008), The radiative susceptibility of cloudy atmospheres to droplet number perturbations: 2. Global analysis from MODIS, *J. Geophys. Res.*, *113*, D14S21, doi:10.1029/2007JD009655.

Penner, J. E., X. Q. Dong, and Y. Chen (2004), Observational evidence of a change in radiative forcing due to the indirect aerosol effect, *Nature*, *427*, 231–234, doi:10.1038/nature02234.

Petters, M. D., and S. M. Kreidenweis (2007), A single parameter representation of hygroscopic growth and cloud condensation nucleus activity, *Atmos. Chem. Phys.*, *7*, 1961–1971, doi:10.5194/acp-7-1961-2007.

Petters, M. D., J. R. Snider, B. Stevens, G. Vali, I. Faloona, and L. M. Russell (2006), Accumulation mode aerosol, pockets of open cells, and particle nucleation in the remote subtropical Pacific marine boundary layer, *J. Geophys. Res.*, *111*, D02206, doi:10.1029/2004JD005694.

Platnick, S., and S. Twomey (1994), Determining the susceptibility of cloud albedo to changes in droplet concentrations with the advanced very high resolution radiometer, *J. Appl. Meteorol.*, *33*, 334–347, doi:10.1175/1520-0450(1994)033<0334:DTSOCA>2.0.CO;2.

Quaas, J., O. Boucher, N. Bellouin, and S. Kinne (2008), Satellite-based estimate of the direct and indirect aerosol climate forcing, *J. Geophys. Res.*, *113*, D05204, doi:10.1029/2007JD008962.

Quaas, J., et al. (2009), Aerosol indirect effects—General circulation model intercomparison and evaluation with satellite data, *Atmos. Chem. Phys.*, *9*, 8697–8717, doi:10.5194/acp-9-8697-2009.

Raes, F. (1995), Entrainment of free tropospheric aerosols as a regulating mechanism for cloud condensation nuclei in the remote marine boundary layer, *J. Geophys. Res.*, *100*, 2893–2903, doi:10.1029/94JD02832.

Ramanathan, V., P. J. Crutzen, J. T. Kiehl, and D. Rosenfeld (2001), Aerosols, climate, and the hydrological cycle, *Science*, *294*, 2119–2124, doi:10.1126/science.1064034.

Roberts, G. C., D. A. Day, L. M. Russell, E. J. Dunlea, J. L. Jimenez, J. M. Tomlinson, D. R. Collins, Y. Shinozuka, and A. D. Clarke (2010), Characterization of particle cloud droplet activity and composition in the free troposphere and the boundary layer during INTEX-B, *Atmos. Chem. Phys.*, *10*, 6627–6644, doi:10.5194/acp-10-6627-2010.

Saide, P. E., et al. (2012), Evaluating WRF-Chem aerosol indirect effects in Southeast Pacific marine stratocumulus during VOCALS-REx, *Atmos. Chem. Phys.*, *12*, 3045–3064, doi:10.5194/acp-12-3045-2012.

Snider, J. R., S. Guibert, J. L. Brenguier, and J. P. Putaud (2003), Aerosol activation in marine stratocumulus clouds: 2. Kohler and parcel theory closure studies, *J. Geophys. Res.*, *108*(D15), 8629, doi:10.1029/2002JD002692.

Snider, J. R., M. D. Petters, P. Wechsler, and P. Liu (2006), Supersaturation in the Wyoming CCN instrument, *J. Atmos. Oceanic Technol.*, *23*, 1323–1339, doi:10.1175/JTECH1916.1.

Stevens, B. (2002), Entrainment in stratocumulus-topped mixed layers, *Q. J. R. Meteorol. Soc.*, *128*, 2663–2690, doi:10.1256/qj.01.202.

Stevens, B., and G. Feingold (2009), Untangling aerosol effects on clouds and precipitation in a buffered system, *Nature*, *461*, 607–713, doi:10.1038/nature08281.

Terai, C. R., R. Wood, D. C. Leon, and P. Zuidema (2012), Does precipitation susceptibility vary with increasing cloud thickness in marine stratocumulus?, *Atmos. Chem. Phys.*, *12*, 4567–4583, doi:10.5194/acp-12-4567-2012.

Tomlinson, J. M., R. Li, and D. R. Collins (2007), Physical and chemical properties of the aerosol within the southeastern Pacific marine boundary layer, *J. Geophys. Res.*, *112*, D12211, doi:10.1029/2006JD007771.

Twomey, S. (1974), Pollution and the planetary albedo, *Atmos. Environ.*, *8*, 1251–1256, doi:10.1016/0004-6981(74)90004-3.

Weber, R. J., and P. H. McMurry (1996), Fine particle size distribution measurements at Mauna Loa Observatory, Hawaii, *J. Geophys. Res.*, *101*, 14,767–14,775, doi:10.1029/95JD02271.

Wood, R. (2006), The rate of loss of cloud droplets by coalescence in warm clouds, *J. Geophys. Res.*, *111*, D21205, doi:10.1029/2006JD007553.

Wood, R., and C. S. Bretherton (2004), Boundary layer depth, entrainment and decoupling in the cloud-capped subtropical and tropical marine

boundary layer, *J. Clim.*, *17*, 3576–3588, doi:10.1175/1520-0442(2004)017<3576:BLDEAD>2.0.CO;2.

Wood, R., C. S. Bretherton, and D. L. Hartmann (2002), Diurnal cycle of liquid water path over the subtropical and tropical oceans, *Geophys. Res. Lett.*, *29*(23), 2092, doi:10.1029/2002GL015371.

Wood, R., K. K. Comstock, C. S. Bretherton, C. Cornish, J. Tomlinson, D. R. Collins, and C. Fairall (2008), Open cellular structure in marine stratocumulus sheets, *J. Geophys. Res.*, *113*, D12207, doi:10.1029/2007JD009371.

Wood, R., M. Köhler, R. Bennartz, and C. O'Dell (2009), The diurnal cycle of surface divergence over the global oceans, *Q. J. R. Meteorol. Soc.*, *135*, 1484–1493, doi:10.1002/qj.451.

Wood, R., et al. (2011), The VAMOS Ocean-Cloud-Atmosphere-Land Study Regional Experiment (VOCALS-REx): Goals, platforms, and field operations, *Atmos. Chem. Phys.*, *11*, 627–654, doi:10.5194/acp-11-627-2011.

Yang, Q., W. I. Gustafson Jr., J. D. Fast, H. Wang, R. C. Easter, H. Morrison, Y.-N. Lee, E. G. Chapman, S. N. Spak, and M. A. Mena-Carrasco (2011), Assessing regional scale predictions of aerosols, marine stratocumulus, and their interactions during VOCALS-REx using WRF-Chem, *Atmos. Chem. Phys.*, *11*, 11,951–11,975, doi:10.5194/acp-11-11951-2011.

Yang, Q., W. I. Gustafson Jr., J. D. Fast, H. Wang, R. C. Easter, M. Wang, S. J. Ghan, L. K. Berg, L. R. Leung, and H. Morrison (2012), Impact of natural and anthropogenic aerosols on stratocumulus and precipitation in the Southeast Pacific: A regional modelling study using WRF-Chem, *Atmos. Chem. Phys. Discuss.*, *12*, 14,623–14,667, doi:10.5194/acpd-12-14623-2012.